Hover Testing of a Small-Scale Rotor with On-Blade Elevons

Mark V. Fulton
Research Scientist

Robert A. Ormiston
Chief Scientist, Aeromechanics

Army/NASA Rotorcraft Division, Aeroflightdynamics Directorate (AMRDEC), US Army Aviation and Missile Command, Ames Research Center, Moffett Field, California

A two-bladed, 7.5-ft diameter dynamic rotor model with 10% chord on-blade elevons driven by piezoceramic bimorph actuators was designed and tested in hover at tip speeds up to 298 ft/s. The elevon actuator succeeded in achieving deflections of ±5 deg at the nominal rotor speed of 760 RPM. Aeroelastic and structural dynamic response characteristics were evaluated over a wide rotor speed range using frequency sweep excitation of the elevon up to 100 Hz. The CIFER® post processing method was very useful for determining frequency response magnitude, phase, and coherence of measured blade root flap bending and torsion moments to elevon input, as well as elevon response to actuator input voltage. Experimental results include actuator effectiveness, effects of low Reynolds number on elevon pitching moments, elevon reversal, and variation of flap bending mode responses with rotor speed and elevon excitation. The active rotor performed satisfactorily and the results provide an encouraging basis for future wind tunnel testing that will evaluate on-blade elevon effectiveness for reducing rotor blade vibratory loads.

Introduction

There has long been a desire to reduce helicopter vibration. Traditional approaches are based on optimizing the rotor and fuselage structure to minimize response to unsteady aerodynamic excitation, or by installing vibration absorbers or isolators in the rotor or fuselage. In recent years increasing attention has been devoted to active higher harmonic control of blade root pitch to reduce vibration at the source. The early work by McHugh and Shaw (Ref. 1) and other investigators used higher harmonic control (HHC) swashplate inputs to drive blade root pitch to attenuate vibratory loads. This technique was very successful in reducing fixed system vibratory loads, but actuator power at high flight speeds and fail-safety considerations have tempered interest in this approach (Ref. 2). Efforts are continuing, however, to apply active swashplate HHC and active pitch link individual blade control (IBC) to benefit rotorcraft performance, vibration, and blade-vortex interaction (BVI) noise, e.g., Refs. 3 and 4.

Use of localized on-blade aerodynamic control concepts is an alternative implementation of individual blade control which is now receiving considerable attention. Although such a concept is certainly not new, as evidenced by the full scale testing of the active servo-flap on the Kaman multi-cyclic controllable twist rotor (MCTR), Ref. 5, on-blade concepts have been revitalized by the promise of newly emerging smart materials (see Refs. 6–9) and hold considerable promise for future advanced rotors. Reference 6 contains an excellent review of active rotor design considerations.

There are two principal methods of implementing on-blade concepts: 1) incorporation of smart materials into the blade structure to control the local twist of the blade—active twist, and 2) actuating a trailing edge control surface, or elevon, to generate local aerodynamic lift and pitching moment—active elevon. The active twist concept is attractive in its simplicity but requires the active material to directly overcome the inherent torsional stiffness of the rotor blade. The active elevon, however, uses aerodynamics as a means to leverage its control authority. The elevon also facilitates the incorporation of multiple controls per blade, providing independent controls to target additional components of the vibratory loads.

Although the force and displacement capabilities of smart materials are limited at the present time, a future implementation of the active elevon concept might provide primary flight control functions of the rotor, eliminating the conventional actuators, swashplate, and blade pitch links (the swashplateless rotor). An idealized configuration (Ref. 10) would also integrate the actuator material into the blade structure, replacing the "conventional" discrete, hinged elevon with a continuously curved surface at the trailing edge of the airfoil, eliminating mechanical linkages and components and thereby improving maintenance and reliability.

Note that the term "elevon" is used herein for simplicity and clarity and to distinguish it from terminology with multiple meanings. For example, "flap" is used for a high-lift device, and for rotor blade flapping motion; "aileron" is used for a roll control surface; and the Kaman "servo-flap" is the external airfoil used to control rotor blade collective and cyclic pitch.

Analytical investigations by Millott and Friedmann, Refs. 11 and 12, and Milgram and Chopra, Ref. 13, indicated that the active elevon control concept has the theoretical potential for reducing rotor vibratory forces and moments. Specifically, with one elevon per blade, and for practical deflection amplitudes, vibration reduction comparable to HHC blade root pitch are achievable. Moreover, the elevon actuator power is significantly less than the HHC power required to pitch the entire blade. These studies also included a preliminary optimization of the structural dynamic properties of the blade, including torsion frequency placement and elevon location.

A number of preliminary design studies have also been conducted to explore the practical feasibility of designing full-scale rotor systems with

Presented at the American Helicopter Society 53rd Annual Forum, Virginia Beach, VA, April 29–May 1, 1997. Manuscript received June 1999; accepted November 2000.

smart material actuators and/or active elevons for reducing rotor vibration and, in some cases, providing primary flight control (Refs. 14, 15).

In recent years a number of efforts have been initiated to investigate and experimentally demonstrate the capabilities of active on-blade control surfaces, primarily using small-scale rotor models in conjunction with smart material actuators. The first design of a bimorph actuator for rotor blade control surface deflection was that of Hall and Spangler (Refs. 16, 17) who conducted a low speed wind tunnel test of a 6.25-in 2-D wing with a piezoceramic bimorph actuator driving a 10%-chord trailing edge elevon. Early 6-ft diameter rotor experiments were reported by Samak and Chopra, and Ben-Zeev and Chopra, Refs. 18 and 19, with piezoceramic bimorphs actuating a 20% chord elevon. These early low-speed rotor tests exhibited problems associated with the limited capacity of the piezoceramic actuators and the mechanical design challenges of incorporating discrete control surface mechanisms in a spinning rotor blade. For example, only limited elevon amplitudes could be achieved and these decreased substantially with rotor speed due to aerodynamic hinge moments as well as friction and linkage losses experienced in the high centrifugal acceleration environment.

With this background, the Aeroflightdynamics Directorate (AFDD) undertook an analytical design study to determine the factors which influence active rotor design. The goal was to develop a configuration that would maximize the aerodynamic effectiveness for a given amount of actuator material subject to the practical constraints of a small-scale model. Piezoceramic materials were found to have a good combination of induced strain, stiffness, and response time. Furthermore, the bimorph concept of Spangler and Hall appeared to offer the potential for developing a practical small-scale research model for exploratory testing at reduced tip-speeds. The objectives of the present research were to develop a rotor blade, elevon, and actuator configuration that would achieve elevon deflections of reasonable amplitude and thereby enable hover and forward flight testing to explore the fundamental aeroelastic and structural dynamic characteristics of rotors with on-blade elevon control surfaces.

Other researchers have made further progress in developing the capability of small-scale model rotors using smart material actuators and on-blade elevons, with some of the most noteworthy testing results presented in Refs. 20 and 21. A DARPA sponsored program is also underway to conduct a flight test demonstration of the capabilities of a full-scale MD-900 helicopter with active on-blade elevons (Ref. 22). Progress has also been made for the alternative active twist concept using integral active fiber composites as reported in Refs. 23 and 24.

The paper will address the design and development of the model rotor blades, including the piezoceramic actuators and elevons, and then present quasi-steady and dynamic test data for nonrotating and rotating conditions in hover. Additional experimental details, particularly regarding actuator design and performance, can be found in the original version of the present paper.

Experimental Model Development

The scope of the present investigation was restricted to a unique, two-bladed, hingeless rotor configuration tested in hover at low tip speeds and low to moderate thrust coefficients. Although the model is not representative of full-scale rotor systems in all respects, the dynamic characteristics are sufficiently representative to permit investigation of many aspects of full-scale systems. The research emphasis is on fundamental structural dynamics characteristics; investigation of rotor performance and nonlinear aerodynamic stall and compressibility effects will require a more sophisticated rotor. The model was not equipped with a closed loop control system—all excitations were open loop. Primary measurements consisted of elevon deflection and blade root flap bending and torsion moments.

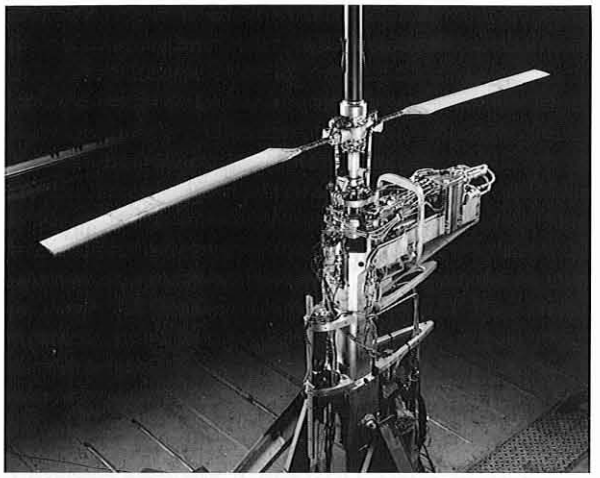

Fig. 1. Rotor installed on the Small Scale Rotor Test Rig in the US Army Aeroflightdynamics Directorate Hover Test Chamber.

For the objectives of a preliminary investigation to explore fundamental behavior, a low tip speed, small-scale dynamic model was acceptable and reduced cost and complexity. The hardware used in this experimental investigation is shown in Figs. 1–3. These figures will be discussed in detail below along with rotor design details and rationale.

Rotor test stand

Hover testing was conducted in the AFDD Hover Test Chamber using the Small Scale Rotor Test Rig (RTR) as shown in Fig. 1. The stand balance system was locked out and not used; no fixed system rotor forces were measured. The existing RTR slip ring was used for instrumentation and an additional slip ring was installed above the rotor hub for supplying electrical power to the lead zirconate titanate (PZT) actuators.

Blade design

In order to reduce model development time and cost, modifications were made to two prototype blades from an existing 7.5-ft diameter Mach-scaled, low-torsion-stiffness hingeless rotor model designed and built for a previous research project (Ref. 25). The resultant rotor blades are untwisted with a rectangular planform and uniform mass and stiffness except at the blade root and the elevon "active section" (see Fig. 2(a)). Chordwise mass and aerodynamic center are located near the quarter chord of the symmetrical NACA 0012 airfoil section. The blades are constructed of composite materials including a fiberglass spar, foam core, and fiberglass wrapped skin construction. Behind the main spar, the upper surface skin and the foam core were removed for installation of an elevon and piezoceramic bimorph actuators at the $0.75R$ location, as shown in Figs. 2(a), 2(b), and 3. Although both the lower surface skin and the access panel were reinforced with balsa wood and fiberglass, the completed active section likely had a degraded strength, suggesting a reduced rotor speed. More importantly, a reduced tip speed lowered the dynamic pressure, thereby enabling useful elevon motions (± 5 deg) for reasonable actuator system mass (34% of the passive blade mass). The general characteristics and properties of the rotor system and blades are given in Table 1.

Elevon-actuator system design

The elevon and actuator configuration included two PZT bimorph actuators driving a single elevon on each blade (Figs. 2(a), 2(b), and 3).

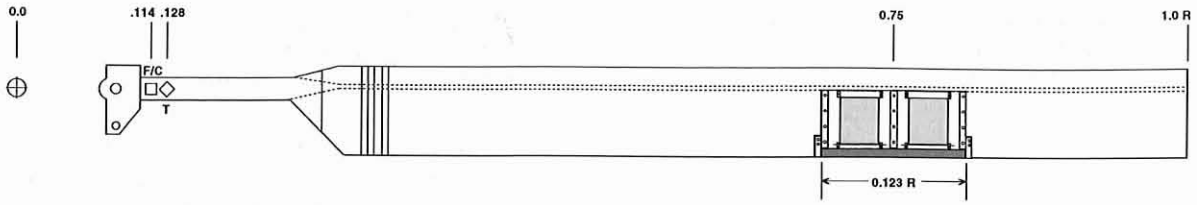

Fig. 2a. Blade planform showing Flap (F), Chord (C), and Torsion (T) strain gage locations on root flexure, as well as transition, constant blade, and active elevon section (approximate scale).

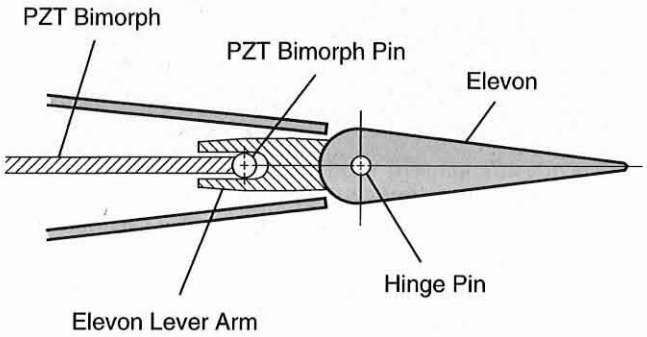

Fig. 2b. Trailing edge of active elevon section showing PZT bimorph bender beam and details of elevon lever arm mechanism (approximate scale).

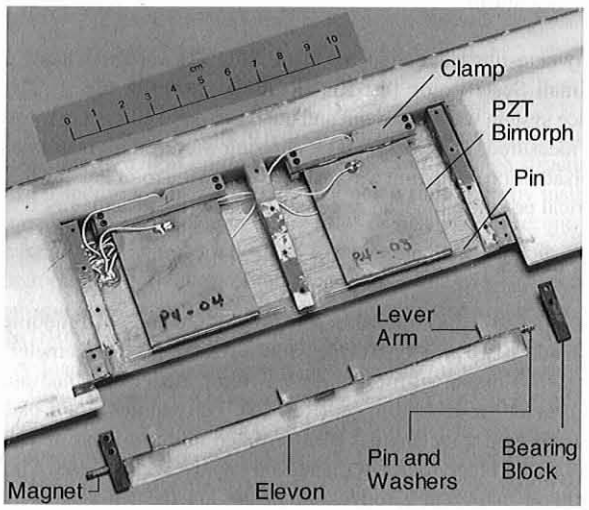

Fig. 3. Active elevon section of the blade with access panel removed and elevon and hinge pin bearing blocks disassembled.

The bimorphs are cantilevered to the rear of the rotor blade main spar. Each bimorph consists of two layers of PZT, straining in opposition to one another, causing a vertical tip deflection which is significantly amplified. The bimorph physics is analogous to the behavior of a bimetallic strip in a thermostat, where electric field plays the role of temperature. A lever arm projects forward from the elevon to engage a pin bonded to the tip of the cantilever PZT beam to produce elevon rotational motion (Fig. 2(b)). The resultant design allows a maximum of approximately ± 10 deg of elevon motion before the elevon lever arms begin to impact the interior of the airfoil cavity.

The design used a 10% chord plain elevon with a span of 12% blade radius, centered at the 75% radial location. The 10% chord elevon was believed to be the smallest practical chord size for providing high aerodynamic efficiency. This choice also yielded a practical lever arm distance,

Table 1. Rotor characteristics & operating conditions

Description	Variable	Value
No. of blades	b	2
Rotor radius	R	45 in (3.75 ft)
Airfoil		NACA 0012
Airfoil chord	c	3.4 in
Elevon chord	c_{elv}	0.34 in (10% c)
Elevon span	S_{elv}	5.55 in (12% R)
Solidity	σ	0.048
Lock no.	γ	5.0
Precone	β_o	0.0
Nominal rotor speed	Ω_o	760 RPM (12.7 Hz)
1st flap mode	$\omega_{\beta 1}$	1.11/rev[a]
1st lag mode	$\omega_{\xi 1}$	1.08/rev[a]
1st torsion mode	$\omega_{\phi 1}$	4.6/rev[a]
Airspeed	V_{tip}; V_{elv}	298; 224 ft/s
Dynamic pressure	q_{tip}; q_{elv}	106; 60 lb/ft^2
Reynolds number	Re_{tip}; Re_{elv}	540,000; 400,000
Mach number	M_{tip}; M_{elv}	0.27; 0.20

[a]Collective pitch = 0 deg, 760 RPM, in air.

thereby allowing the use of commercially available PZT bimorphs to match actuator stiffness with aerodynamic stiffness. The 75% radial location was not specifically chosen to maximize response of any particular flap bending mode—it was simply chosen as a suitable, representative location for exploratory testing. This actuator/elevon system was designed to provide ± 5 deg elevon motion at an airspeed of 270 ft/s and low frequencies.

An important design goal was to minimize both unwanted friction forces and free play in the bimorph-elevon mechanism. To achieve this goal, considerable attention was devoted to the design and construction of the elevon hinge, "lever" mechanism, and bimorph clamp (see Figs. 2(b) and 3). The elevon was hinged at its two ends using steel elevon hinge pins bonded to the elevon and mounted in low friction Delrin® bearing blocks. The bearing blocks were bolted to the blade, and a brass and Teflon® thrust washer pair was used to support the elevon centrifugal force exerted against the outboard Delrin® bearing block. To reduce bimorph-to-elevon "lever" mechanism friction, steel pins bonded to the ends of the PZT bimorphs engaged slotted fiberglass elevon lever arms. The lever arm slots accommodated small chordwise translations of the bimorph pins. The root of each bimorph was bonded inside a fiberglass-epoxy sandwich, which was bolted in place to prevent movement within the clamp (see Fig. 3). Finally, adjustments were made to the alignment of the PZT bimorphs and the bearing blocks to minimize friction and binding.

Bimorph actuator details

The bimorphs were purchased from Piezo Systems, Inc. and were trimmed in length from the Standard 2-Layer Piezoelectric Motor Element T220-A2-501. The standard width of 1.5 in was retained but

the length was reduced to 2.05 in (including 0.25 in for clamping). These bimorphs are made from two piezoceramic 5A layers, each 0.0075 in thick, bonded on either side of a metallic center shim. The combined thickness is 0.020 in. The bimorphs were poled for parallel configuration and had nickel electrodes. A semicircular hole was ground at the edge of the upper 5A layer to permit access to the center shim. This actuator was specified by the manufacturer to provide a blocked force of 1.6 oz and a free deflection of ± 0.048 in for a free length of 2 in when ± 180 V_{DC} (12 V/mil) is applied.

Electrical excitation

The bimorphs in each blade were electrically connected in parallel. Each bimorph pair was powered by a Trek Model 50/750 High Voltage, Solid-State Amplifier. The sinusoidal AC command voltage input to the Trek was produced by a function synthesizer. This voltage was either a single frequency (from 5 to 100 Hz) or a logarithmic frequency sweep (1–105 Hz in 27 s). The maximum AC voltage applied was 110 Vrms (14.7 Vrms/mil). The AC voltage was superimposed on a DC voltage used to bias the bimorph layers in the direction of their polarization to avoid depolarization by the relatively large AC voltage. Each bimorph pair was powered through a separate Trek channel, although both channels were driven by the same AC voltage command. At times, one blade was given a different DC bias in order to help compensate for blade-to-blade differences in mean elevon position.

Instrumentation, data acquisition, and processing

Elevon motion was measured with a Hall-effect transducer. The accompanying magnet was poled through its diameter and was bonded to the inboard elevon bearing pin to rotate with the elevon. Blade response was measured through full strain gage bridges at the root flexure of each blade. The flap and chord strain gage bridges were at $0.114R$, and the torsion strain gage bridge was at $0.128R$ (see Fig. 2(a)). In addition, the pitch of blade 1 was measured with a potentiometer. Both PZT voltage and current were measured. The PZT power leads and the elevon Hall-effect transducer power and signal leads were routed from the hub to the active section on the lower surface of the blade, with the PZT wires placed near the quarter chord, and the Hall-effect wires 0.5 in forward of the trailing edge.

Analog six-pole Bessel filters were used with a -3 dB cut-off frequency of 100 Hz. All of the transducers were sampled and digitized. The dynamic data was acquired at a sample rate of 543 Hz (43/rev at 760 RPM). Dwell tests were sampled for 7.5 s while logarithmic frequency sweeps were sampled for 30 s.

Analysis of the acquired time histories was performed using an in-house program for the dwell tests. This program was used to display the time histories, extract their means, and obtain the frequency content using a Fast Fourier Transform (FFT). For the frequency sweeps, however, frequency response functions (FRFs) were obtained using CIFER® (Comprehensive Identification from FrEquency Responses), Refs. 26 and 27. The CIFER® module FRESPID (Frequency RESPonse IDentification) was used to obtain the FRFs for five different spectral window lengths. Generally, FRESPID was used to concatenate two 30 s time histories for each of the reported cases. Finally, the CIFER® module COMPOSITE was used to perform multi-window averaging of the FRESPID results, thus providing more accurate FRF evaluations for a wide frequency range. These COMPOSITE results are reported in this paper.

The FRFs are presented for either individual blades or for the "average" blade. The averaged results represent the collective, or symmetric, rotor mode for a two-bladed rotor. Averaging the measurements reduces some of the antisymmetric noise sources and small fixed system interactions, and averages the effects of blade differences.

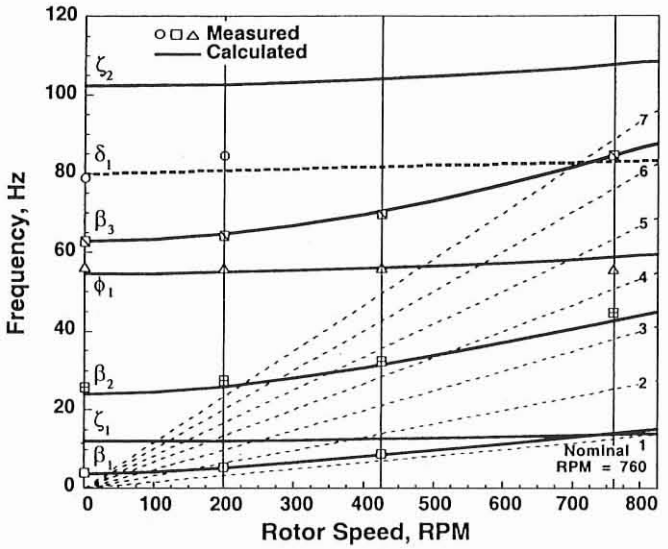

Fig. 4. Rotor blade frequencies versus rotor speed in air.

Rotor and elevon natural frequencies

The elevon and rotor blade frequencies in the rotating system, in air, are shown in Fig. 4 as a function of rotor speed. The nominal operating speed is 760 RPM (12.7 Hz). The solid, smooth curves are analytical predictions of the Second Generation Comprehensive Helicopter Analysis System (2GCHAS, Ref. 28), at 0 deg collective pitch, using blade properties adjusted to match measured nonrotating frequencies. Rap tests revealed the nonrotating blade frequencies to be 3.66, 12.0, and 55.6 Hz for flap, chord, and torsion, respectively. The discrete symbols indicate the natural frequencies obtained from frequency sweeps performed at four rotor speeds (0, 200, 425, and 760 RPM) at 3.5 deg collective pitch. Since the blades include the added mass of the elevon actuators and were originally designed for higher tip speed operation, some of the bending frequencies are somewhat different from typical full scale characteristics. At nominal rotor speed the first flap bending (β) frequency is typical for hingeless rotors (1.11/rev). The first lead-lag (ζ) frequency of 1.08/rev is relatively close to 1/rev. The nominal rotor speed also results in a somewhat unconventional second flap bending mode above 3/rev; this mode is typically below 3/rev. The combination of low torsion stiffness and low rotor speed results in a reasonable first torsion (ϕ) frequency of 4.6/rev. Both the first elevon/actuator (δ) and third flap bending frequencies are between 6/rev and 7/rev. The elevon/actuator frequency was calculated assuming quasi-static 2-D airfoil conditions and ignoring mechanical friction. The frequency was predicted to be 80 Hz for zero airspeed and to increase slightly with rotor speed.

Experimental Testing and Results

The model was tested over a range of rotor speeds including 0, 200, 425, and 760 RPM (marked on Fig. 4) and thus yielded a variety of dynamic characteristics. At 425 RPM the principal nondimensional frequencies are much increased (relative to 760 RPM)—the second flap and first torsion frequencies are above 4/rev and 7/rev, respectively. While not representative of typical rotor blades, these alternative natural frequencies afforded a useful opportunity to broaden the fundamental understanding of on-blade elevon control and vibration reduction characteristics.

All experimental results in this paper are for a collective pitch of 3.5 deg. The cyclic pitch was approximately zero; that is, no attempt was made to minimize the 1/rev flapping. Elevon motion tests were performed

using dwell tests (from 5 to 100 Hz) or logarithmic frequency sweeps (1–105 Hz in 27 s). Quasi-steady data was taken at a low frequency of 5 Hz to facilitate data acquisition and to minimize the effects of static friction and instrumentation zero drift. Finally, the voltage level was varied to investigate aeroelastic nonlinearities.

The results of experimental testing will be presented in sequence, first examining quasi-steady characteristics of the system (for low frequency elevon excitation), for a range of rotor speeds. Next, results from frequency sweeps will be presented to highlight the behavior of this structural dynamic/aeroelastic system. Although elevon deflections will be shown, the primary emphasis will be on the resultant blade flap bending and torsion moments.

Quasi-steady results from dwell tests

Actuator effectiveness. The basic measure of the effectiveness of the PZT bimorph is the ability of this actuator to produce the desired elevon deflection (±5 deg) under full centrifugal and aerodynamic forces. Rotating tests of the present design showed that elevon deflection performance was quite good. Typical results for elevon deflection over a range of operating rotor speeds are shown in Fig. 5 for several levels of 5 Hz AC excitation voltage. At the nominal 110 Vrms PZT excitation, elevon deflections exceeding ±6 deg were achieved at 760 RPM.

A design prediction, included in Fig. 5 as a solid line, shows a gradual decrease in elevon deflection with rotor speed as a result of the increasing elevon aerodynamic hinge moment. This prediction used a PZT voltage of 64 Vrms instead of the (anticipated) nominal voltage of 110 Vrms in order to provide voltage margin to accommodate unmodeled effects such as elevon bearing friction, aerodynamic damping, and PZT hysteresis. Experimental data, shown as discrete symbols and curve fits, is included for the two blades at two voltage levels of 75 and 110 Vrms. The experimental trend matches the prediction—elevon angle varies in proportion to $1/(1+KU^2)$, where U is the relative wind speed and K is a constant of proportionality. The voltage margin allowed during the design was adequate—the elevon motion exceeded ±6 deg at 760 RPM for the nominal voltage of 110 Vrms. Thus, the elevon deflections are considered satisfactory for present purposes.

As shown in Fig. 5, the low voltage PZT excitation (75 Vrms) was applied over the full rotor speed range. At low rotor speed, the actuator motion approached the mechanical constraint of the airfoil cavity (approximately ±10 deg). Consequently, the application of the nominal voltage (110 Vrms) was restricted to 300 RPM and above. It may also be noted that the elevon performance differs between the two blades; it is presumed that aerodynamic, electro-mechanical, and friction differences between the two elevons and the PZT bimorphs are responsible.

Elevon effectiveness: Torsion moment response. Given that a PZT actuator is successful in producing sufficient elevon deflection, it is of interest to examine the effectiveness of the elevon in producing blade aerodynamic lift and pitching moment. For untwisted blades at low collective pitch, the measured blade root torsion moment directly reflects the aerodynamic pitching moment produced by elevon deflection. The measured torsion moment response versus the elevon deflection amplitude is shown in Fig. 6 for 5 Hz excitation at 760 RPM. Note that the results are linear for both blades except at small elevon deflections, where there are substantial differences between blades. These differences most likely reflect elevon and airfoil contour differences at the two active sections.

If the moment response is normalized by the corresponding elevon amplitude, a measure of elevon torsion effectiveness is obtained. The normalized torsion moments for both blades are plotted as a function of rotor speed in Fig. 7 (for 75 and 110 Vrms) and show quadratic behavior reflecting an elevon aerodynamic pitching moment proportional to dynamic pressure. At higher rotor speeds, the tennis racket effect increases, and the torsion response moderates. This moderation, however, is not pronounced for the range of rotor speeds tested.

The measured elevon effectiveness in Fig. 7 is significantly lower than would be anticipated based on thin airfoil theory. This may be illustrated using Eq. (A-5) from the simplified rigid-blade analytical model developed in the Appendix. Results based on several values of the pitch moment derivative ($c_{m\delta}$) are shown in Fig. 7. Using the thin airfoil theory value for a 10% chord plain flap (0.55/rad) yields elevon torsion effectiveness that significantly exceeds the measured results.

The reason for the difference is presumed to be, in part, the effects of the low Reynolds number (Re) of $\sim 4.0 \times 10^5$ at the blade elevon radial position. It is well known that airfoil lift characteristics even at low angles of attack are moderately influenced at such low Re, but there is very little data available for airfoil pitching moment from trailing edge

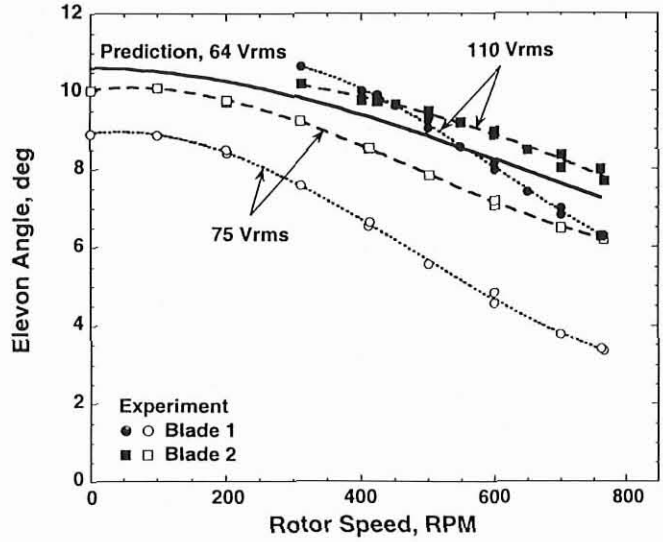

Fig. 5. Elevon actuator effectiveness, elevon deflection amplitude versus rotor speed, 5 Hz excitation.

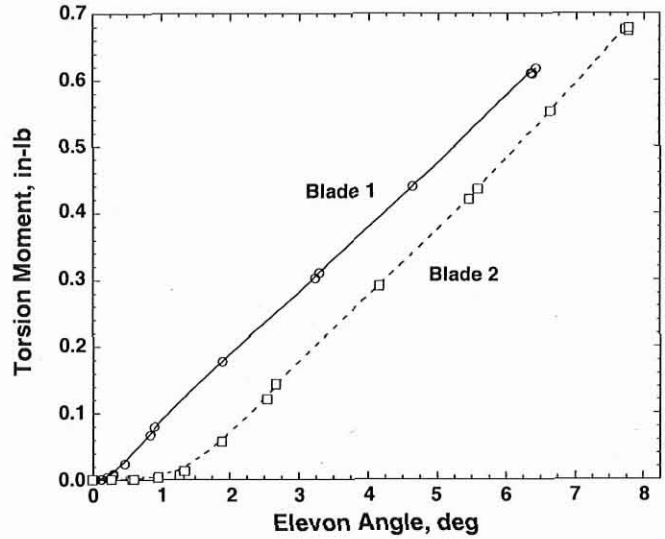

Fig. 6. Blade root torsion moment amplitude versus elevon deflection, 5 Hz, 760 RPM.

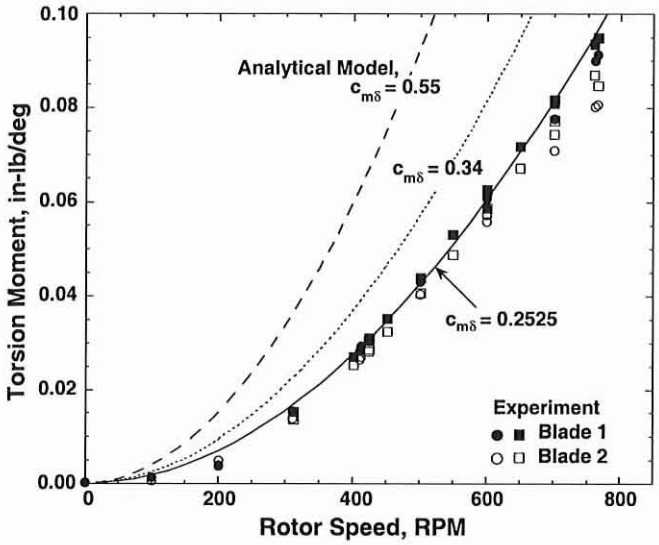

Fig. 7. Elevon torsion moment effectiveness versus rotor speed, 5 Hz.

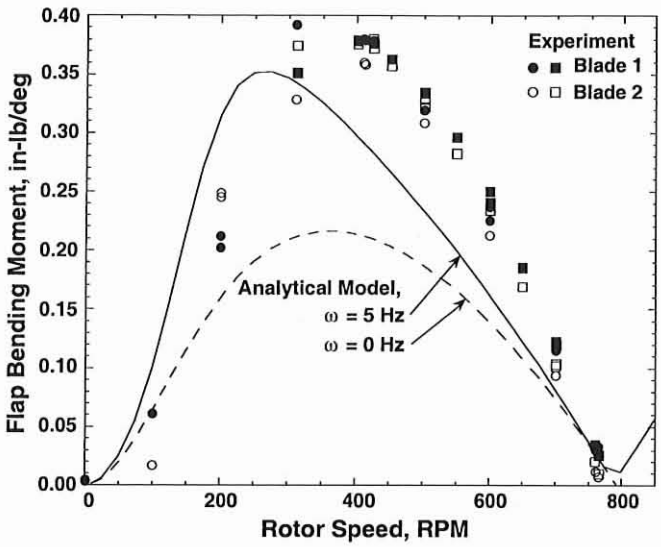

Fig. 8. Elevon flap bending moment effectiveness versus rotor speed, 5 Hz—"elevon reversal" effect.

flap deflection at such low Re. Limited data for a 12.5% symmetrical RAF 30 airfoil (Ref. 29) at $3.6 \times 10^5 Re$ suggests that the aerodynamic pitching moment response to trailing edge flap deflection is about 60% of the magnitude predicted by inviscid thin airfoil theory. Using a value for $c_{m\delta} = 0.34$/rad yields an improvement in Fig. 7, although the measured results are still overpredicted. Further reduction of the elevon pitching moment coefficient to $c_{m\delta} = 0.2525$/rad produced a good fit to the experimental data.

In an attempt to further explore the reduced elevon aerodynamic pitching moment, modifications to the elevon shape were undertaken. These modifications included thickening the trailing edge analogous to a Gurney flap, sealing the elevon-to-blade hinge gap, and increasing the trailing edge angle by adding a series of progressively thicker wedges to increase the thickness at the trailing edge of the elevon. The trailing edge wedges did, in fact, increase the elevon aerodynamic effectiveness by up to 59%. Such major shape alterations are not proposed as practical means of improving elevon effectiveness, but were investigated to explore a simple means of offsetting a possible drawback of small-scale, low Reynolds number testing.

An associated measure of elevon effectiveness is the tip torsion deflection. Using the simplified rigid blade analytical model (Eq. A-5), the value of $|\phi/\delta| = 0.064$ is obtained at 760 RPM when using the theoretical elevon derivative $c_{m\delta} = 0.55$/rad. For a 5 deg elevon deflection, this yields $\phi = 0.32$ deg tip torsion deflection. At the torsion mode natural frequency, the amplitude is increased by roughly a factor of five (see discussion below); thus the maximum torsion deflection would be $\phi \sim 1.6$ deg. Note, however, that these are ideal values and the elevon effectiveness of the present small-scale model was considerably reduced for the reasons discussed above.

Elevon effectiveness: Flap bending response. Analogous to quasi-steady elevon-torsion effectiveness, it is of interest to examine the corresponding elevon flap bending effectiveness. Results for blade root flap bending, normalized by the elevon deflection, are shown in Fig. 8 as a function of rotor speed for the 5 Hz "quasi-steady" excitation frequency. Interestingly, the elevon flap bending effectiveness increases roughly quadratically at low rotor speed but then approaches a peak value at approximately 450 RPM before diminishing to near zero at 760 RPM. It is apparent that the direct aerodynamic lift produced by the elevon deflection ($c_{l\delta}$) is being overcome, as the rotor speed increases, by the indirect lift ($c_{l\alpha}$) due to blade twist induced by elevon pitching moment ($c_{m\delta}$). This culminates in "elevon reversal" slightly above 760 RPM; the physical mechanism is analogous to aileron reversal on fixed wing aircraft, which is caused by insufficient wing torsional rigidity for operation at high flight speeds.

The simplified quasi-steady analytical blade model developed in the Appendix may be used to confirm and help explain this behavior. Equation (A-6) was used to calculate the steady-state (0 Hz elevon deflection) flap bending moment response using elevon aerodynamic coefficients of $c_{l\delta} = 1.13$/rad and $c_{m\delta} = 0.2525$/rad. The analytical result is qualitatively similar to the measured results in Fig. 8 including the phenomenon of elevon reversal. Quantitatively, however, the analytical model underpredicts the measurements. In Ref. 30, the simplified analytical model was extended to include flap bending and torsion dynamics and subsequently used to generate results for 5 Hz elevon excitation that are also included in Fig. 8. This significantly improves the correlation and confirms that blade flap bending dynamics are significant even for relatively low elevon excitation frequencies.

The simplified analytical model in the Appendix was used to determine an expression for the elevon reversal rotor speed, as defined by the condition when the flap bending elevon effectiveness vanishes (reverses sign), Eq. (A-7). The elevon reversal speed was shown to be proportional to the nonrotating torsion frequency and, for typical conventional full-scale rotor blades, the elevon reversal speed is on the order of the rotor speed.

The importance of the elevon reversal speed depends on the intended functional purpose of the on-blade elevon control. For active control of rotor loads, vibration, and blade-vortex interaction noise, which involve excitation frequencies of 3, 4, 5/rev or above, the higher frequency blade bending and torsion structural dynamics are probably more important than the static elevon reversal phenomenon. Active control of rotor performance involving 2/rev excitation may be relatively more sensitive to the elevon reversal speed. However, using on-blade elevon control surfaces for primary flight control (replacing the conventional swashplate collective (0/rev) and cyclic (1/rev) pitch inputs at the blade root) will directly involve elevon reversal characteristics. Rotor control effectiveness will require maximizing elevon flap bending effectiveness of the blade (for low frequencies) and this will require a very low elevon reversal speed and thus a very low torsion frequency (low torsional stiffness). A

familiar example is the Kaman servo-flap controlled rotor. It should be noted that a principal barrier for using smart materials actuators for such a "swashplateless rotor" is that the required blade pitch angles (15–20 deg) exceed the capability of current smart material actuators.

Dynamic results from frequency sweeps

Among the most fundamental characteristics of an active rotor system are the inherent, or open loop, dynamic response characteristics of the actuator, elevon, and rotor blade aeroelastic system. These characteristics were a principal area of interest for the present investigation. In this section the results of dynamic testing will be presented including representative examples for blade root flap bending, root torsion, and elevon deflection for various rotor speeds. At the outset, it might be noted that the presence of an aerodynamic control surface mounted on the blade *in the rotating system* provides a unique opportunity to study the aeroelastic and structural dynamic characteristics of a rotor blade, as will be evident from the results to be presented here.

Dynamic response characteristics were primarily determined using a logarithmic frequency sweep of the elevon actuator input voltage. An example of the resulting elevon time history, along with the corresponding blade moments, is given in Fig. 9 for a nonrotating condition. The frequency is swept from 1 to 105 Hz in 27 s. The responses of the flap bending and torsion moment exhibit resonances when the input excitation sweeps across the bending and torsion mode natural frequencies. Frequency Response Functions (FRFs) of the input-output were calculated from the time histories using CIFER® (Comprehensive Identification from FrEquency Responses), Refs. 26 and 27. Dynamic response data are presented for blade-averaged data as described earlier, except for elevon deflection, which is always presented for blade 2. The system

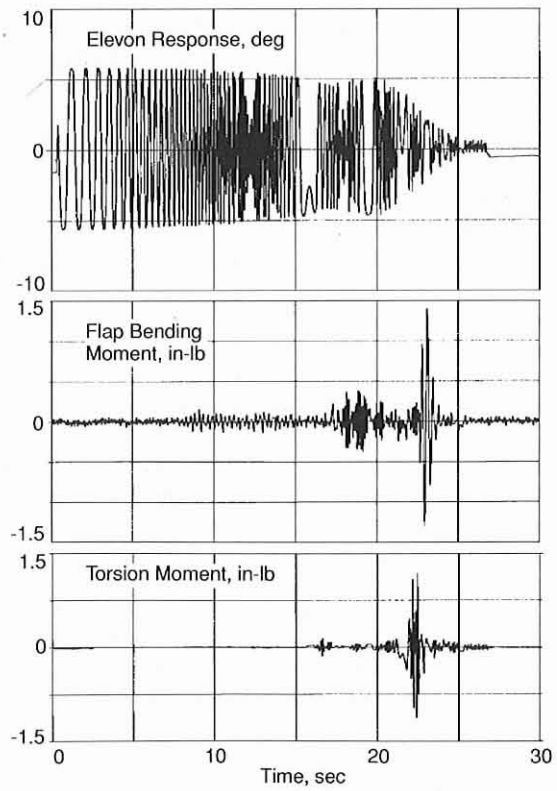

Fig. 9. Example of response to sine sweep excitation used for calculation of frequency response functions.

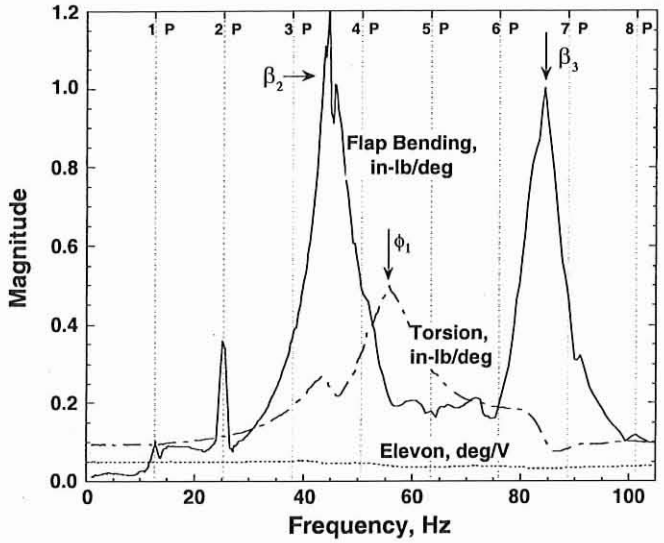

Fig. 10. Frequency response functions, 2-blade average (except blade 2 for elevon response), RPM = 760.

natural frequencies for the flap (β), torsion (ϕ), and elevon (δ) modes are marked on the figures.

Nominal rotor speed (760 RPM). Frequency response measurements for the rotor operating at 760 RPM are now discussed. The magnitude of three frequency response functions (FRFs) are shown in Fig. 10: 1) flap bending moment per unit elevon deflection input, 2) torsion moment per unit elevon deflection input, and 3) elevon deflection per unit PZT voltage input. Each of the three curves gives a clear indication of the structural dynamic/aeroelastic behavior of the corresponding mode up to a maximum frequency of about 100 Hz (8/rev).

First, consider the flap bending moment response. At this rotor speed, a principal characteristic of the flap moment FRF are the resonant peaks at the second and third flap bending modes (3.5/rev and 6.7/rev, respectively). Here, the second flap mode response is larger than the third mode. The first flap bending mode, however, is barely evident because this mode is largely eliminated by the proximity of this rotor speed to the elevon reversal speed. Interestingly, there is no evident influence of the torsion mode (4.4/rev) on flap bending. This is somewhat unexpected since a change in blade angle of attack from elastic twist should affect flap bending. Even without a clear effect on the flap bending moment, however, the effect of torsion may still be important. Further interpretation of this behavior will require comparisons with analytical predictions. The torsion response to elevon deflection in Fig. 10 exhibits the expected behavior of a damped, single degree of freedom, second order system, peaking at the torsion mode natural frequency (56 Hz). In addition, the torsion response shows an apparent coupling with the neighboring second flap bending mode. Finally, the elevon response shown in Fig. 10 shows no resonant peak and decreases with increasing frequency. Qualitatively different behavior will be later shown for other rotor speeds.

It may be noted that strain gage measurements were taken only at the blade root; consequently, response variations along the blade span, that may influence the behavior of the blade root response, cannot be observed. Finally, note the near absence of n/rev noise response except at the 1 and 2/rev frequencies. For the in-phase (collective) elevon inputs used during the frequency sweep, dynamic inflow and wake effects on blade lift and flap bending moment will be present only at even n/rev excitation frequencies. These effects, however, should not be large due to operation at a non-zero thrust condition.

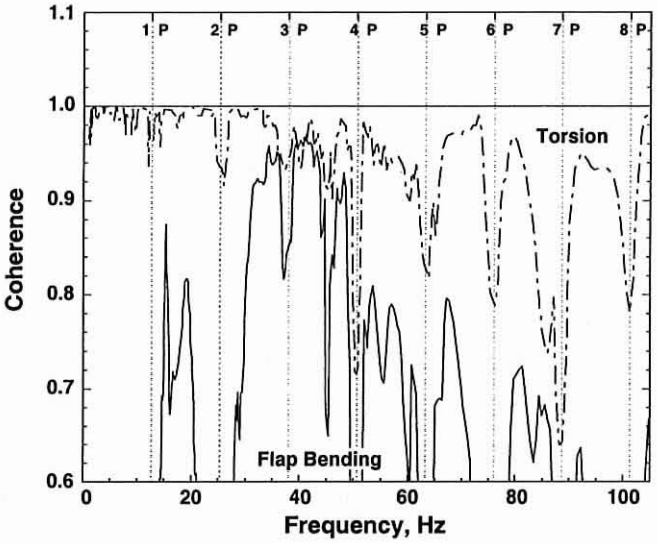

Fig. 11. Coherence of frequency response functions for flap bending and torsion moments, 2-blade average, RPM = 760.

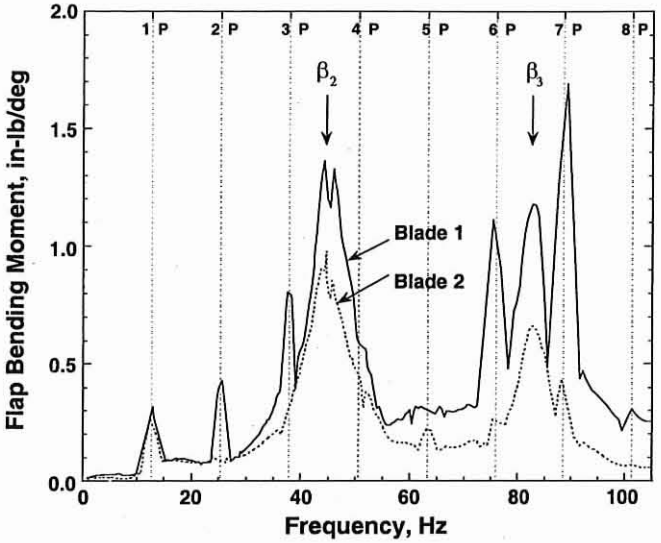

Fig. 12. Blade-to-blade variation in flap bending moment frequency response function magnitude, RPM = 760.

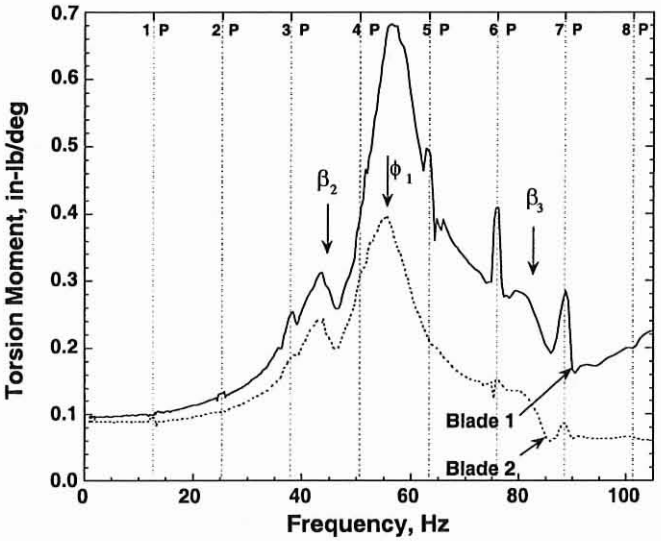

Fig. 13. Blade-to-blade variation in blade root torsion moment frequency response function magnitude, RPM = 760.

The coherence of the flap bending and torsion moment FRFs is shown in Fig. 11. The floor of the figure is set at an "acceptable" coherence of 0.6, which corresponds to a random error of 4–12%. "Good" results are achieved once the coherence reaches 0.85, which corresponds to a random error of 2–6%. The coherence for the torsion moment is generally good, while that for the flap bending moment is, in general, only acceptable. As previously noted, the n/rev aerodynamic "noise" present in the test environment contaminates the FRFs; this contamination is indicated by large "valleys", or rapid reductions in the coherence at the n/rev frequencies. In addition, the coherence function "plateaus" decrease as the elevon frequency increases. This trend is largely due to a decreased amplitude of elevon motion at higher frequencies, which produces a lower signal-to-noise ratio. (The decreasing elevon amplitude is an artifact of the electrical circuit design which reduces the PZT voltage at higher frequencies.) Additional testing demonstrated that coherence improvements could be achieved by using either a higher voltage level or a smaller frequency range (like 30–105 Hz); these tests generally increased the height of the coherence plateaus and reduced the width of the n/rev valleys. The overall quality of the FRFs is closely related to the elevon's control authority, with lower random error for larger elevon motions due to the increased signal-to-noise ratio.

A few results will now be presented to illustrate the extent to which the FRFs of the individual blades differ from one another. Figures 12 and 13 present the magnitude of flap bending moment and torsion moment FRFs for both blades. The basic character of the responses is very similar, although there are significant differences in magnitude for the two blades. Note that the effect of the n/rev periodic noise is considerably more prominent in these FRFs than for the averaged data previously shown in Fig. 10.

Rotor speeds from 0 to 760 RPM. A useful way to better understand the dynamic blade response characteristics to elevon excitation is to observe the evolution of the frequency response functions (FRFs) as the rotor speed varies from zero to the nominal RPM. Several figures are presented for this purpose, combining results for four different rotor speeds: 0, 200, 425, and 760 RPM.

First, Fig. 14 shows the FRF magnitude of elevon deflection to PZT voltage for blade 2. The elevon dynamic response at 0 RPM strongly reflects the mechanical dynamics of the system and reveals a resonant peak at about 80 Hz. The strong effect of aerodynamic loads is clear in the damped peak response of the actuator-elevon mode for higher rotor speeds. In addition, the reduction of the quasi-steady (i.e., low frequency) elevon deflection is also clear and reflects the dynamic pressure effect previously shown in Fig. 5. Analytical predictions indicated that the natural frequency of the elevon should not change significantly with rotor speed (see Fig. 4), although this can not be verified from Fig. 14. The elevon/voltage FRF for blade 1 did not exhibit a significant resonance, even at 0 RPM. The cause of this is not known but is presumably due to poor mechanical characteristics of the actuator/elevon combination.

The FRF magnitude of torsion moment to elevon deflection is shown in Fig. 15. Again, the main features are evident: the strong increase in quasi-steady elevon effectiveness (at low frequencies, as in Fig. 7), the near invariance of torsion (ϕ) mode natural frequency (about 56 Hz) with rotor speed, and the interactions with the second and third flap bending (β) modes as marked on the figure.

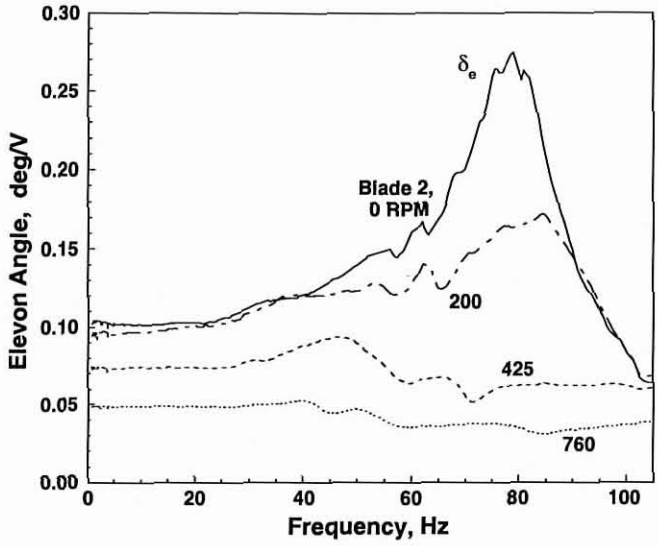

Fig. 14. Variation with rotor speed of elevon deflection frequency response function magnitude (blade 2).

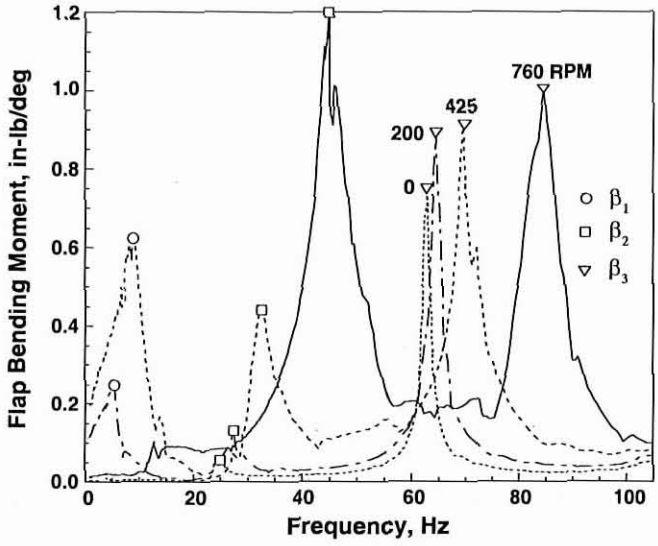

Fig. 16. Variation with rotor speed of blade root flap bending moment frequency response function magnitude (2-blade average).

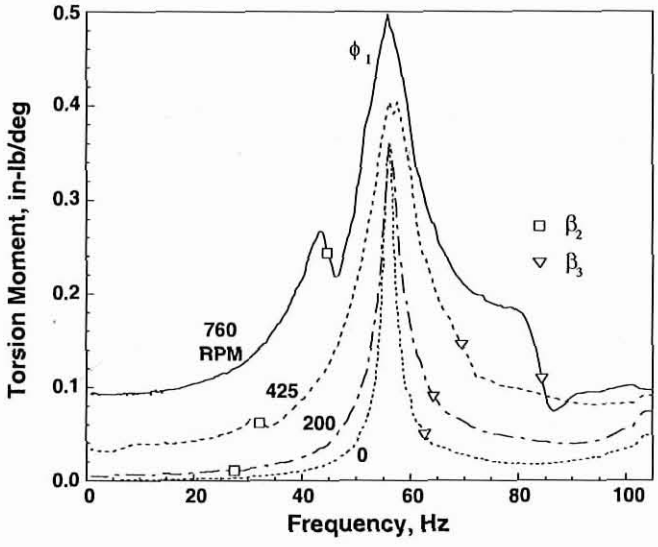

Fig. 15. Variation with rotor speed of blade root torsion moment frequency response function magnitude (2-blade average).

It is also of interest to infer the relative influence of the two primary sources of excitation of the root torsion moment, namely the aerodynamic pitching moment of the elevon and the inertial pitching moment of the PZT beam and elevon. If the aerodynamic excitation were assumed constant with frequency, then the torsion response at any rotor speed would largely be that of a damped, single degree of freedom, second order system. At first glance, it appears that the peak response at 760 RPM is simply the peak at 0 RPM plus the quasi-steady response at 760 RPM. This occurrence is deceptive, however, since the aerodynamic damping at 760 RPM is substantially higher than the structural damping at 0 RPM. In fact, it appears that at 760 RPM the majority of the peak response is caused by the aerodynamic excitation of the elevon.

The FRF magnitude of flap bending moment to elevon deflection is shown in Fig. 16. As would be expected, the effects of rotor speed and aerodynamics are very strong. Aerodynamics is particularly important for the second flap bending mode, as the resonant peak increases roughly by a factor of 20 from 0 to 760 RPM. The third flap bending mode is not nearly as sensitive. The first flap bending mode is the most complex because of its proximity to the quasi-steady elevon reversal phenomenon. In particular, this resonant peak increases between 0 and 425 RPM; it has nearly vanished by 760 RPM due to the onset of elevon reversal (previously shown in Fig. 8). The influence of elevon reversal on the first flap bending mode was explored in greater detail in Ref. 30.

These results further illustrate that the effectiveness of active elevon control for loads and vibration reduction will depend strongly on the specific dynamic properties of the rotor blade at the important excitation frequencies present in forward flight. Additional analysis (particularly of the FRF phase measurements) will be needed to determine the relative importance of the elevon lift effect and the pitching moment effect.

Concluding Remarks

A small-scale rotor was successfully tested in hover to explore the basic aeroelastic and structural dynamic characteristics of a rotor blade equipped with a 10% chord elevon control surface envisioned for eventual use as a means to benefit rotorcraft vibration, performance, and BVI noise. The principal findings are summarized as follows:

1) The practical feasibility of using piezoceramic bimorph actuators to provide reasonable elevon deflections was demonstrated for a small-scale, reduced tip-speed model. Elevon deflections in excess of ± 10 deg and ± 5 deg were achieved at rotor speeds of 0 and 760 RPM, respectively.

2) Elevon deflection amplitude was shown to decrease with rotor speed in a manner consistent with the increase in aerodynamic hinge moment due to dynamic pressure.

3) Low-frequency blade root torsion moment response to elevon deflection was found to increase with rotor speed as expected. Elevon torsion effectiveness, however, was lower than predicted by thin airfoil theory, mainly due to the effects of low Reynolds number on elevon control power, $c_{m\delta}$.

4) Low-frequency blade root flap bending response to elevon deflection was found to increase due to direct lift of the elevon ($c_{l\delta}$) as rotor speed increased but then decreased due to the opposing indirect lift ($c_{l\alpha}$) from elastic blade twist induced by the negative aerodynamic pitching moment of the elevon ($c_{m\delta}$), leading toward elevon reversal slightly above 760 RPM.

5) Frequency response measurements indicated that blade root torsion moment increased in conventional fashion to peak at the torsion natural frequency of about 56 Hz (4.4/rev) at 760 RPM. At resonance, torsion moment response was amplified approximately five times the steady-state amplitude.

6) Blade root flap bending moment frequency response measurements clearly showed the large dynamic amplification due to elevon excitation near the natural frequencies for the 2nd and 3rd flap bending modes.

7) Frequency sweep excitation proved to be an efficient experimental technique for measuring rotor blade frequency response characteristics. This technique should be suitable for broader application to rotorcraft aeroelasticity and structural dynamics.

Appendix: Simplified Rigid Blade Analytical Model

The simplified analytical model used for comparison and interpretation of the elevon torsion and flap bending effectiveness measurements is briefly outlined here. The cantilever elastic blade is modeled as a rigid body with steady-state flap (β) and torsion (ϕ) rotations about spring restrained hinges located at the center of rotation for specified elevon deflection (δ). The model uses quasi-steady 2-D strip theory aerodynamics with zero inflow and without any unsteady wake effects. The blade aerodynamic torsion and flap hinge moments, M_{ϕ_a} and M_{β_a}, are obtained by integrating the blade lift and moment along the blade length.

$$M_{\phi_a} = -\frac{\gamma I_\beta \bar{c}\Omega^2}{6}\left[A_3 \frac{c_{m\delta}}{a}\delta\right] \tag{A-1}$$

$$M_{\beta_a} = \frac{\gamma I_\beta \Omega^2}{8}\left[\phi + A_4 \frac{c_{l\delta}}{a}\delta\right] \tag{A-2}$$

where γ is the blade Lock number, I_β is the flapping inertia, a is the airfoil lift curve slope, and $c_{l\delta}$ and $c_{m\delta}$ are the lift and moment coefficient derivatives for elevon deflection. The dimensionless chord is defined as $\bar{c} = c/R$ and Ω is the rotor angular velocity. The elevon geometry constants A_3 and A_4 are defined in terms of the inboard and outboard radii of the elevon, r_i and r_o, as follows:

$$A_3 \equiv \left(\bar{r}_o^3 - \bar{r}_i^3\right) \quad \text{and} \quad A_4 \equiv \left(\bar{r}_o^4 - \bar{r}_i^4\right) \tag{A-3}$$

The aerodynamic moments may be equated to the customary centrifugal and hinge spring moments:

$$M_{\phi_a} = \left(K_\phi + I_\phi \Omega^2\right)\phi \quad \text{and} \quad M_{\beta_a} = \left(K_\beta + I_\beta \Omega^2\right)\beta \tag{A-4}$$

where K_β and K_ϕ are the flap and torsion hinge spring constants, and I_β and I_ϕ are the blade flap and torsion inertias. These equations may be used to obtain closed form solutions for the steady-state torsion and flap bending response normalized by elevon deflection:

$$\frac{\phi}{\delta} = -\frac{\gamma}{6}\frac{\bar{c}}{\bar{I}_\phi} A_3 \frac{c_{m\delta}}{a}\left[\frac{\Omega^2}{\Omega^2 + \omega_\phi^2}\right] \tag{A-5}$$

$$\frac{\beta}{\delta} = \frac{\gamma}{8p^2} A_4 \frac{c_{l\delta}}{a}\left[1 - \frac{\Omega^2}{B\left(\Omega^2 + \omega_\phi^2\right)}\right] \tag{A-6}$$

where $p^2 = 1 + \omega_\beta^2/\Omega^2$, $\omega_\beta^2 = K_\beta/I_\beta$, $\omega_\phi^2 = K_\phi/I_\phi$, $\bar{I}_\phi = I_\phi/I_\beta$, and

$$B = \frac{6\bar{I}_\phi}{\gamma \bar{c}}\left(\frac{A_4}{A_3}\right)\frac{c_{l\delta}}{c_{m\delta}}$$

These equations may be used to determine the elevon reversal speed (Ω_R), that is defined by the condition when the flap bending response vanishes (reverses sign). Equation (A-6) may be solved to yield

$$\Omega_R = \sqrt{\frac{B}{1-B}}\,\omega_\phi \tag{A-7}$$

The elevon reversal rotor speed is shown to be proportional to the nonrotating torsion frequency, ω_ϕ. The parameter B is proportional to the ratio of the elevon lift and moment coefficient derivatives, $c_{l\delta}$ and $c_{m\delta}$, and the elevon constants A_4 and A_3. For blades with typical inertia properties and elevon geometry similar to the present model, B is generally much less than unity and thus the elevon reversal speed varies with the square root of B. For typical full-scale rotor blades, the elevon reversal speed is on the order of the nominal rotor speed.

For the numerical results included in Figs. 7 and 8, the torsion and blade root flap bending moments were calculated using Eqs. (A-5) and (A-6) multiplied by the respective values for torsion and flap bending spring stiffness to convert deflections to moments. The following physical property values were used for the calculations: $\gamma = 6.0$, $\omega_\beta = 0.293\Omega_o$, $\omega_\phi = 4.34\Omega_o$, $a = 2\pi$, $I_\phi/I_\beta = 0.000921$, $A_3 = 0.1758$, and $A_4 = 0.1763$. The remaining parameter values are given in Table 1. For the 5 Hz flap bending moment results in Fig. 8, the inertial and aerodynamic damping terms were included (Ref. 30).

Acknowledgments

The authors would like to thank Mr. David L. Sharpe for engineering guidance and assistance in preparing and conducting the hover test. They would also like to acknowledge the significant contributions of the entire test team. Finally, the authors gratefully acknowledge the outstanding effort of Mr. Terry L. Fish in fabricating the active elevon blades.

References

[1]McHugh, F. J., and Shaw, J., Jr., "Benefits of Higher-Harmonic Blade Pitch: Vibration Reduction, Blade Load Reduction, and Performance Improvement," American Helicopter Society Mideast Region Symposium on Rotor Technology, Essington, PA, August 1976.

[2]Miao, W., Kottapalli, S. B. R., and Frye, H. M., "Flight Demonstration of Higher Harmonic Control (HHC) on S-76," American Helicopter Society 42nd Annual Forum, Washington, D.C., June 2–5, 1986.

[3]Yu, Y. H., Gmelin, B., Heller, H., Philippe, J. J., and Preisser, J. S., "HHC Aeroacoustic Rotor Test at the DNW—The Joint German/French/US Project," Twentieth European Rotorcraft Forum, Amsterdam, The Netherlands, October 4–7, 1994.

[4]Jacklin, S. A., Blass, A., Swanson, S. M., and Teves, D., "Second Test of a Helicopter Individual Blade Control System in the NASA Ames 40-by 80-Foot Wind Tunnel," American Helicopter Society 2nd International Aeromechanics Specialists' Conference, Bridgeport, CT, October 11–13, 1995.

[5]McCloud, J. L., III, and Weisbrich, A. L., "Wind Tunnel Test Results of a Full-Scale Multicyclic Controllable Twist Rotor," American Helicopter Society 34th Annual Forum, Washington, D.C., May 15–17, 1978.

[6]Strehlow, H., and Rapp, H., "Smart Materials for Helicopter Rotor Active Control," AGARD/SMP Specialist's Meeting on Smart Structures for Aircraft and Spacecraft, Lindau, Germany, October 1992.

[7]Chopra, I., "State-of-the-Art of Smart Structures and Integrated Systems," SPIE Smart Structures and Materials Conference, San Diego, CA, February 1996.

[8]Crawley, E. F., and de Luis, J., "Use of Piezoelectric Actuators as Elements of Intelligent Structures," *AIAA Journal*, Vol. 25, (10), October 1987.

[9]Loewy, R. G., "Recent Developments in Smart Structures with Aeronautical Applications," 37th Israel Annual Conference on Aerospace Sciences, Tel Aviv, Haifa, Israel, February 1997.

[10]Ormiston, R. A., "Can Smart Materials Make Helicopters Better?," Fourth Workshop on Dynamics and Aeroelastic Stability Modeling of Rotorcraft Systems, College Park, MD, November 1991.

[11]Millott, T. A., and Friedmann, P. P., "Vibration Reduction in Helicopter Rotors Using an Active Control Surface Located on the Blade," 33rd AIAA/ASME/ASCE/AHS/ASC Structures, Structural Dynamics, and Materials Conference, Dallas, TX, April 1992.

[12]Millott, T. A., and Friedmann, P. P., "Vibration Reduction in Helicopter Rotors Using an Actively Controlled Partial Span Trailing Edge Flap Located on the Blade," NASA CR 4611, June 1994.

[13]Milgram, J., and Chopra, I., "Helicopter Vibration Reduction with Trailing Edge Flaps," American Helicopter Society 2nd International Aeromechanics Specialists' Conference, Bridgeport, CT, October 11–13, 1995.

[14]Straub, F. K., and Charles, B. D., "Preliminary Assessment of Advanced Rotor/Control System Concepts (ARCS)," USA AVSCOM TR 90-D03, August 1990.

[15]Fenn, R. C., Downer, J. R., Bushko, D. A., Gondhalekar, V., and Ham, N. D., "Terfenol-D Driven Flaps for Helicopter Vibration Reduction," *Smart Materials and Structures*, Vol. 5, (1), February 1996.

[16]Hall, S. R., and Spangler, R. L., "Piezoelectric Helicopter Blade Flap Actuator," US Patent No. 5,224,826, July 1993.

[17]Spangler, R. L., and Hall, S. R., "Piezoelectric Actuators for Helicopter Rotor Control," 31st AIAA/ASME/ASCE/AHS/ASC Structures, Structural Dynamics and Materials Conference, Long Beach, CA, April 1990.

[18]Samak, D. K., and Chopra, I., "A Feasibility Study to Build a Smart Rotor: Trailing Edge Flap Actuation," SPIE Smart Structures and Materials Conference, Albuquerque, NM, February 1993.

[19]Ben-Zeev, O., and Chopra, I., "Advances in the Development of an Intelligent Helicopter Rotor Employing Smart Trailing-Edge Flaps," *Smart Materials and Structures*, Vol. 5, (1), February 1996.

[20]Prechtl, E. F., and Hall, S. R., "Hover Testing of a Mach-Scaled Rotor with an Active Trailing Edge Flap," Eighth ARO Workshop on the Aeroelasticity of Rotorcraft Systems, State College, PA, October 1999.

[21]Koratkar, N. A., and Chopra, I., "Wind Tunnel Testing of a Mach-Scaled Rotor Model with Trailing-Edge Flaps," American Helicopter Society 56th Annual Forum, Virginia Beach, VA, May 2–4, 2000.

[22]Straub, F. K., "Development of a Full Scale Smart Rotor System," Eighth ARO Workshop on the Aeroelasticity of Rotorcraft Systems, State College, PA, October 1999.

[23]Rodgers, J. P., and Hagood, N. W., "Hover Testing of a 1/6th Mach-Scale CH-47D Blade with Integral Twist Actuation," Proceedings of the 9th International Conference on Adaptive Structures and Technologies, Cambridge, MA, October 1998.

[24]Wilbur, M. L., Yeager, W. T., Jr., Wilkie, W. K., Cesnik, C. E. S., and Shin, S.-J., "Hover Testing of the NASA/Army/MIT Active Twist Rotor Prototype Blade," American Helicopter Society 56th Annual Forum, Virginia Beach, VA, May 2–4, 2000.

[25]Maier, T. H., Sharpe, D. L., and Lim, J. W., "Fundamental Investigation of Hingeless Rotor Aeroelastic Stability, Test Data and Correlation," American Helicopter Society 51st Annual Forum, Fort Worth, TX, May 9–11, 1995.

[26]Tischler, M. B., and Cauffman, M. G., "Frequency-Response Method for Rotorcraft System Identification: Flight Applications to BO-105 Coupled Rotor/Fuselage Dynamics," *Journal of the American Helicopter Society*, Vol. 37, (3), July 1992.

[27]Tischler, M. B., Driscoll, J. T., Cauffman, M. G., and Freedman, C. J., "Study of Bearingless Main Rotor Dynamics from Frequency-Response Wind Tunnel Test Data," American Helicopter Society Aeromechanics Specialists Conference, San Francisco, CA, January 19–21, 1994.

[28]Rutkowski, M. J., Ruzicka, G. C., Ormiston, R. A., Saberi, H., and Jung, Y., "Comprehensive Aeromechanics Analysis of Complex Rotorcraft Using 2GCHAS," *Journal of the American Helicopter Society*, Vol. 40, (4), October 1995.

[29]Jacobs, E. N., and Pinkerton, R. N., "Pressure Distributions Over a Symmetrical Airfoil Section with Trailing Edge Flap," NACA Report No. 360, 1930.

[30]Ormiston, R. A., and Fulton, M. V., "Aeroelastic and Dynamic Rotor Response with On-Blade Elevon Control," 24th European Rotorcraft Forum, Marseilles, France, September 15–17, 1998.